Journal of Materials Chemistry C

ROYAL SOCIETY OF CHEMISTRY

PAPER

View Article Online
View Journal

Cite this: DOI: 10.1039/d5tc02343b

A novel [2.2]paracyclophane bridged tris(2,4,6-trichlorophenyl)methyl-diradical and its interaction with circularly polarized light

Larissa Schöneburg,[a] Mona E. Arnold,[a] Mario R. Rapp,[b] Rémi Blinder,[c] Markus Gross,[a] Julia Zolg,[ad] Fedor Jelezko,[cd] Holger F. Bettinger *[b] and Alexander J. C. Kuehne *[ad]

Received 17th June 2025,
Accepted 29th October 2025

DOI: 10.1039/d5tc02343b

rsc.li/materials-c

Chiral diradicals that interact with light represent interesting molecules with potential applications in quantum technology. Here, we report the synthesis of such a novel tris(2,4,6-trichlorophenyl)methyl derived diradical, which is coupled to a chiral bis-acetylene [2.2]paracyclophane using Sonogashira cross-coupling. Its optical properties are compared with those of a non-chiral [2.2]paracyclophane diradical homologue and a phenylacetylene tris(2,4,6-trichlorophenyl)methyl radical reference compound. We study the weak electronic and magnetic interactions between the two unpaired electrons and the chiroptical properties of the diradicals. The enantiomers of the chiral diradical are separated *via* chiral HPLC and studied by circular dichroism. Magnetic characterization reveals triplet state population, due to near-degenerate singlet–triplet energy levels with a vanishingly small splitting ($\Delta E_{ST} < 0.1$ kJ mol^{-1}), consistent with the results from DFT calculations.

Introduction

Molecules with two interacting and unpaired electrons are of special interest for quantum technological applications, for example, in quantum sensing of magnetic fields.[1,2] Recently, optically distinguishable electronic spin isomers have been demonstrated in a stable organic diradical, further underlining the potential of such systems for quantum material research.[3] Moreover, dyes that interact with circularly polarized light have become an essential tool for various sensing scenarios in the life sciences.[4] While chiral units can be easily incorporated into molecules with closed electronic shells, the design of chiral diradicals is a more challenging endeavour. Key problems in diradical design and synthesis remain in overcoming incomplete conversion to the diradical and achieving high stability in the resulting radical centers.[5,6]

Stable open-shell molecules – radicals – have long been of interest, due to their unique electronic and photophysical properties. Among them, tris(2,4,6-trichlorophenyl)methyl (TTM) radicals are particularly well-studied, known for their remarkable stability and doublet emission characteristics.[7–10] Their robustness arises from the propeller-like conformation of the phenyl rings, where the chlorine atoms screen the hemispheres above and below the radical center, effectively preventing dimerization.[11] The photoluminescence of TTM radicals has been explored extensively, especially in the context of tuning the optical properties through substitution with different electron donating moieties and their impact on the photoluminescence quantum yield (ϕ).[12,13]

While monoradical TTM species are well understood, the growing interest in TTM-derived diradicals introduces new challenges and opportunities. A notable example is the TTM–TTM Chichibabin diradical, which exhibits a significant red-shift in its emission band compared to TTM monoradicals. This shift has been attributed to enhanced conjugation, with emission originating from the lowest excited state, in accordance with Kasha's rule, albeit with only a modest ϕ of approximately 1%.[14,15] Another intriguing TTM diradical is the *para*-connected TTM-Ph-TTM Müller hydrocarbon, characterized by a singlet ground state with a thermally accessible triplet state.[16] Such systems exemplify how subtle structural modifications tune electron spin interactions in organic diradicals.[17–19] Recent computational studies on yet elusive TTM-Ph-Ph-TTM reveal a singlet ground state as well as an unexpected blue-shift in emission, likely due to the increased

[a] *Institute of Macromolecular and Organic Chemistry, Ulm University, Albert-Einstein-Allee 11, 89081, Ulm, Germany. E-mail: alexander.kuehne@uni-ulm.de*
[b] *Institut für Organische Chemie, Eberhard Karls Universität Tübingen, Auf der Morgenstelle 18, 72076, Tübingen, Germany. E-mail: holger.bettinger@uni-tuebingen.de*
[c] *Institute of Quantum Optics, Ulm University, Albert-Einstein-Allee 11, 89081, Ulm, Germany*
[d] *Center for Integrated Quantum Science and Technology, Ulm University, Albert-Einstein-Allee 11, 89081, Ulm, Germany*

distance between the radical centers.[20] A particularly compelling objective is the realization of a TTM-based diradical with a true triplet ground state. To date, *meta*-connected TTM-Ph-TTM has remained the only example of TTM derivatives exhibiting such behavior, while this *meta*-connectivity prevents quinoidal conjugation and plays a crucial role in favoring the triplet ground state.[21] Interestingly, many [2.2]paracyclophanes (PCPs), including those in which each phenyl ring is only functionalized once, can also prevent quinoid formation. The connectivity through such PCPs where the individual phenyl rings are only mono-functional is therefore termed pseudo-*geminal*, -*ortho*, -*meta* and -*para*.[22] Moreover, apart from through-space conjugation,[23] no real electron delocalization (and formation of a quinoidal structure) is possible (see Fig. 1).[17,24–27] The coupling between the TTM units and the PCP can be performed *via* Sonogashira cross-coupling, ensuring a sufficient distance between the radical centers by introducing rigid ethynyl-spacers (PCP-A), obviating steric stresses in the diradical, and thus minimizing undesired radical recombination (see Fig. 1).[17,28] In the case of pseudo-*o*-PCP-A, this structural approach introduces an additional intriguing property, namely, planar chirality, endowing the pseudo-*o*-PCP coupled TTM-diradicals with unique chiroptical properties and potentially opening new pathways for designing stable and tunable diradical systems (see Fig. 1).[24,25]

Chiral radicals with chiroptical properties have been explored in TTM-based monoradicals, by introducing chiral electron donor units. The configurational stability and photostability of helicene-based radicals enable their enantiomeric separation *via* chiral HPLC, facilitating precise studies of their interaction with circularly polarized light.[29,30] While the TTM radical exists in a propeller geometry and therefore automatically exhibits chirality, the TTM propeller enantiomers can interconvert and racemize quickly at room temperature, obviating the application of TTM as a chiroptical material.[31] Only a few chiral diradicals are known. A related (dichloropyridyl) bis(trichlorophenyl) methyl radical (PyBTM) has been linked with a binaphthyl unit exhibiting axial chirality.[32] Another example reported is a double helical aminyl diradical exhibiting a pronounced triplet ground state.[33] However, to date, TTM-derived diradicals with a stable chiral connector and their potentially interesting properties have remained unknown.

In this study, we present the synthesis of a chiral pseudo-*ortho*-bis-ethynylene paracyclophane bridged TTM diradical (pseudo-*o*-PCP-TTM_2) and a non-chiral pseudo-*para*-bis-ethynylene paracyclophane bridged TTM diradical (pseudo-*p*-PCP-TTM_2). As a reference compound, we also synthesize the respectively related phenylethynylene-TTM monoradical (Ph-TTM) (see Fig. 1). We compare the spectral properties of the chiral and non-chiral diradicals and the circular dichroism (CD) of the enantiomerically resolved pseudo-*o*-PCP-TTM_2. While the pseudo-*p*-PCP-TTM_2 with oppositely positioned TTM radicals and the phenylethynylene-TTM radical exhibit a similar doublet signal in the electron paramagnetic resonance (EPR) spectrum, the chiral pseudo-*o*-PCP-TTM_2 diradical exhibits zero-field splitting, resulting from dipolar interaction between the two radical centres.

These findings establish PCP-based diradicals as a promising platform for chiral diradicals with the ability to deliberately control the electron spin interactions.

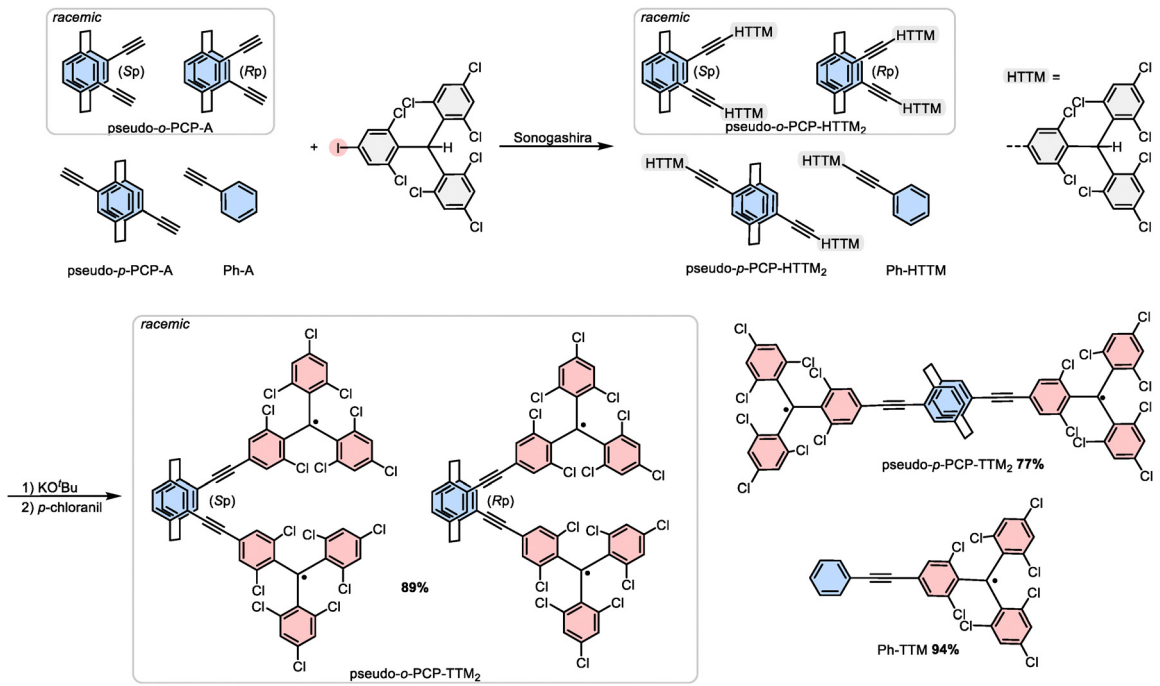

Fig. 1 Synthesis of the chiral (planar chirality, S_p and R_p) and non-chiral TTM-diradical compounds, as well as the monoradical reference compound phenylacetylene-TTM *via* Sonogashira cross-coupling.

Results and discussion

Synthesis

To synthesize our chiral and non-chiral TTM-diradicals, we start from pseudo-*o*-PCP-A and pseudo-*p*-PCP-A (their synthesis is described elsewhere).[34] In addition, we employ phenylacetylene representing one half of the bis-ehtynylene-PCP bridge. We connect the racemic chiral and non-chiral bis-acetylene PCPs and phenylacetylene to the closed-shell iodine-functionalized HTTM radical precursor using Sonogashira cross-coupling (see Fig. 1).[26,35] For the conversion of the closed-shell precursors to the radicals and diradicals, the widely established deprotonation-oxidation mechanism using KO^{t}Bu and *p*-chloranil is repeated three times for the diradicals to maximize the diradical conversion, until no more monoradical impurities are observed in high-resolution mass spectrometry (HRMS).[8]

While Pd-catalyzed cross-coupling reactions such as Suzuki coupling can be used to directly couple the TTM-radical to other conjugated units without losing the open-shell character, Sonogashira coupling provides only the closed-shell product, even when we start from the open-shell iodo-TTM radical. To rule out the conceivable reduction of the TTM radical by the copper co-catalyst, we also tested a copper-free Pd-catalyzed Sonogashira reaction protocol (see the Experimental section in the SI).[36] Interestingly, even in this copper-free approach, the product is also the closed-shell PCP-HTTM$_2$ radical precursor in a yield of 95%, requiring once again the deprotonation–oxidation cycle after Sonogashira coupling for the conversion to the diradicals. Beneficially, we can make use of the closed-shell pseudo-*o*-PCP-HTTM$_2$ as a reference compound and as an isosteric closed-shell matrix to "dilute" the diradicals in the solid state.

Magnetic characterization and DFT geometry optimization

We investigate the magnetic properties of the novel radicals by EPR spectroscopy (see Fig. 2). In flash-frozen toluene solution and polymethyl methacrylate (PMMA), we observe a strong central EPR signal for all samples, similar to the signal of a monoradical ($g \approx 2$), which either indicates incomplete conversion of the precursor to the diradical or the formation of radical–radical associates (π-dimers or higher aggregates) (see Fig. S2 and S3 in the SI). In such aggregates, the majority of electron spins can couple antiferromagnetically, leaving a small fraction of individual electron spins that produce the apparent monoradical-like signal.[37,38] We do not assume σ-dimerization of the chlorinated trityl units, which is suppressed in these systems.[39] This problem of aggregation can be reduced when

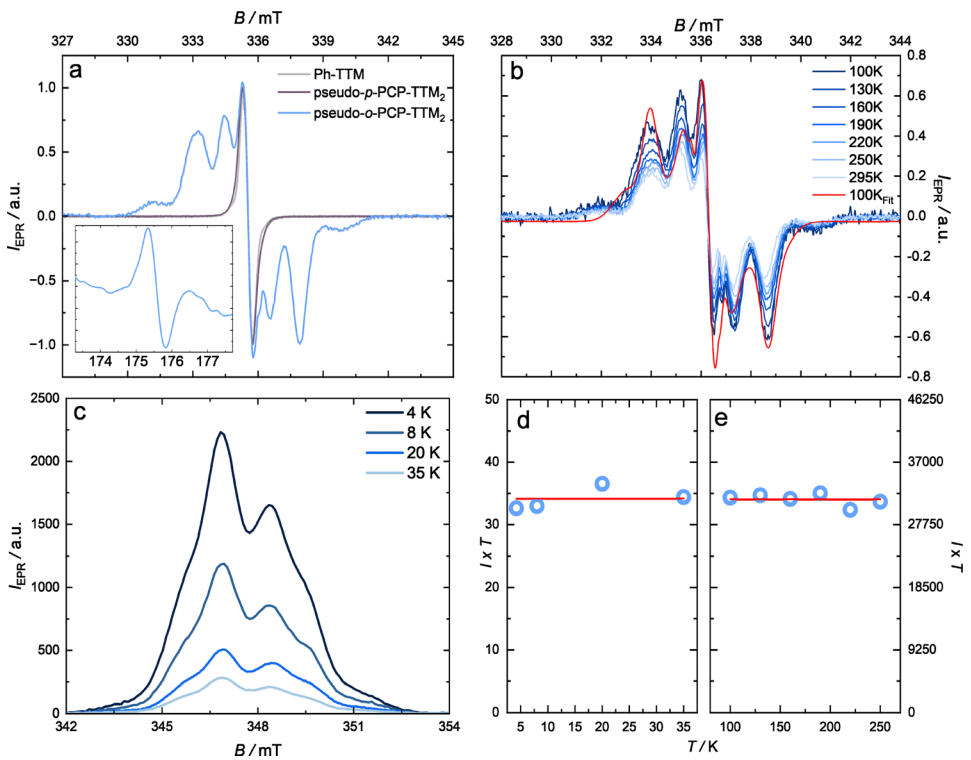

Fig. 2 (a) Comparison of the continuous wave (cw-)EPR spectra of the pseudo-*o*-PCP-TTM$_2$ with phenylacetylene-TTM and pseudo-*p*-PCP-TTM$_2$ at 190 K in their respective isosteric matrices. The inset shows the signal of pseudo-*o*-PCP-TTM$_2$ at half-field. (b) cw-vt-EPR measurements of pseudo-*o*-PCP-TTM$_2$ (0.05 wt%) in the precursor (pseudo-*o*-PCP-HTTM$_2$) matrix and fitting of the experimental data at 100 K using EasySpin to extract magnetic parameters. (c) Pulsed EPR spectra of pseudo-*o*-PCP-TTM$_2$ (0.05 wt%) in the radical precursor (pseudo-*o*-PCP-HTTM$_2$) matrix in the temperature range of 4 K to 35 K (helium). (d) Pulsed EPR signal intensity multiplied by temperature ($I \times T$) as a function of temperature (4 K to 35 K) of pseudo-*o*-PCP-TTM$_2$ with a constant model fit. (e) cw-EPR signal intensity multiplied by temperature ($I \times T$) as a function of the temperature (100 K to 295 K) of pseudo-*o*-PCP-TTM$_2$ with a constant model fit.

we employ the diradicals in a matrix of their closed-shell (respective HTTM) precursor. To obtain this "solid solution" (of the radicals in their precursors), we dissolve the respective closed-shell precursor and the (di)radicals in benzene and then remove the solvent by freeze-drying, providing us with the solid powder. This solid solution allows for measurements in the solid state at room temperature, while the self-similar molecular geometry of the precursor and the radical prevents aggregation. For pseudo-*o*-PCP-TTM$_2$ in its isosteric matrix, we observe zero-field splitting (ZFS) in the EPR spectrum, indicating dipolar interactions between the unpaired electrons (see Fig. 2a). The sharp central peak is much reduced, corroborating that it is not a result of monoradical impurities but rather due to the formation of aggregates, as hypothesized above (*cf.* Fig. 2a with Fig. S2 and S3). As indicated above, we could not detect any residual monoradical after synthesis by HRMS, further substantiating the claim that a certain amount of formed aggregates is responsible for the sharp central signal (see HRMS spectra in Fig. S23, SI). In contrast, both pseudo-*p*-PCP-TTM$_2$ and phenylacetylene-TTM (Ph-TTM) show signals of a doublet ground state in the EPR spectrum (see Fig. 2a). While this doublet is natural for the Ph-TTM monoradical, the signal is also reasonable when considering the larger inter-spin distance in the pseudo-*p*-PCP-TTM$_2$, indicating that the molecule is a biradical, in which the spin-centers act independently as doublets. In contrast, the diradical character of pseudo-*o*-PCP-TTM$_2$ is further corroborated by the formally forbidden transition with $|\Delta m_s| = 2$ at half field (see the inset in Fig. 2a). For extracting magnetic parameters such as the dipolar coupling constant $|D/hc|$ and the symmetry of the spin density distribution $|E/hc|$, we simulate the spectra (using EasySpin), which allows us to determine the electronic and structural properties and the relative occupation of the triplet sublevels (population distribution), which influences the spectral shape (see Fig. 2b).[40,41] The experimental data for pseudo-*o*-PCP-TTM$_2$ can be fitted with a single diradical species and a central component with spin $S = 0.5$, representing the signal from aggregates (see Fig. S4 in the SI). To verify these data, we turn to density functional theory (DFT) at the UB3LYP/def2-TZVP level of theory for structural optimization and to relate the geometry to the magnetic properties. We perform a conformational analysis *via* DFT for the R_p isomer, which reveals three distinct diradical species, differentiated by the rotational configuration of the TTM propeller units (see the SI, Table S1 and Fig. S10 and 11; the S_p isomer exhibits the same energies as its respective mirror-imaged stereoisomers). The most stable R_p-based diastereomer is the one with the trityl propellers in the (+,+) conformation, whereas the (+,−) and (−,−) diastereomers are less stable by 12.22 kJ mol^{-1} and 15.48 kJ mol^{-1}, respectively (see Fig. S10). Such a large gap excludes significant populations of higher-energy species, justifying the fit of the experimental EPR data with a single diradical species. However, we would like to point out that the EPR analysis is performed in the solid solution (of the diradicals in a matrix of their closed shell homologue), whereas the DFT calculations are performed in the gas phase. The difference between the experimentally determined EPR data and the fitted spectrum might arise from matrix stabilization of the other diastereomers or of conformers or dimers not predicted by the gas-phase calculations. The DFT geometry optimization reveals a distance of $d = 0.75$ nm between the radical centers (for all diastereomers) (see Fig. S10 in the SI). These values are in the same range as the spin–spin distances obtained from the experimental $|D/hc|$ values using the dipolar coupling equation,[42,43] giving $d = 0.80$ nm. The dihedral angle between the p-orbitals (θ_{pp}) will influence the strength of the dipolar coupling. The (+,+) diastereomer, calculated as being the most stable, has the smallest $\theta_{pp} = 28.2^\circ$, resulting in an almost parallel alignment of the p-orbitals (see Fig. S10a). For the interpretation of the pseudo-*p*-PCP-TTM$_2$ EPR spectrum, the chirality of the TTM propellers appears to be irrelevant, since the distance between the radical centers is large at 1.9 nm and the calculated single point energies are independent of the (+) or (−)-conformation of the TTM propellers (see Table S2 and Fig. S15, SI). Fitting of the EPR spectra allows us to determine the strength of the dipolar coupling in pseudo-*o*-PCP-TTM$_2$ through the ZFS parameters $|D/hc| = 85$ MHz and $|E/hc| = 14$ MHz (see Table 1). The relatively large value of $|E/hc|$ indicates that the spin density distribution is non-symmetrical along the axis of maximum dipolar coupling.[44]

Table 1 Summary of the photophysical, geometrical, and EPR properties: g is the Landé central splitting factor (anisotropic), $|D/hc|$ and $|E/hc|$ are the ZFS parameters, d is the distance between the spin-centers, θ_{pp} is the dihedral angle between the p-orbitals at the two spin-centers, λ_{abs} is the maximum absorption wavelength, λ_{PL} is the maximum photoluminescence wavelength, and ϕ is the photoluminescence quantum yield

	$g_{x,y,z}$ (aniso.)	$\lvert D/hc\rvert$/MHz	$\lvert E/hc\rvert$/MHz	d/nm[a]	θ_{pp}/°[a]	λ_{abs}/nm	λ_{PL}/nm	ϕ/%
pseudo-*o*-PCP-TTM$_2$	2.0030, 2.0024, 2.0045	85	14	0.80	28.2	314 375 436	688	0.9
pseudo-*p*-PCP-TTM$_2$	2.0038			1.92		300 375 440	660	0.8
Ph-TTM	2.0033					375 413	620	1.2

[a] Calculated from the DFT optimized molecular geometries.

Finally, we note that chiral diradicals can, in principle, present a non-zero antisymmetric coupling of the form $(S_1 \times S_2) \times d$, arising from the spin–orbit interaction.[45,46] However, adding this coupling in the spectral simulation does not improve the fit, suggesting that the antisymmetric interaction is negligible.

The obtained *g*-factors are close to the value of 2.0036 as is typical for TTM diradicals (see Table 1).[14,16] The deviation from the *g*-factor of a free radical electron, with g_e = 2.0023, is because of the orbital angular momentum, in other words the spin–orbit coupling, which is larger for states near degeneracy.[47]

To better understand the nature of the ground state of pseudo-*o*-PCP-TTM$_2$, we perform variable-temperature (vt-)EPR spectroscopy using both pulsed and continuous wave (cw) techniques. Pulsed EPR measurements are carried out at helium temperatures (4 K to 35 K, see Fig. 2c), while cw-EPR spectroscopy is used in the temperature interval from 100 K to 295 K (see Fig. 2b). Although both methods are suitable in principle, cw-EPR spectroscopy suffers from strong microwave power saturation at low temperatures, making pulsed EPR spectroscopy the method of choice in this range. This saturation effect suggests that one of the relaxation times (T_1 or T_2) increases as the temperature decreases.[48] T_2 was measured by varying the interpulse delay (τ) in a two-pulse electron spin echo experiment, yielding a value of T_2 = 2 μs after fitting it with a biexponential decay function $I(2\tau) = \exp\left(\frac{-2\tau}{T_2}\right)$ (see Fig. S6 in the SI). Apparently, T_2 is limited by hyperfine interactions with nearby protons.[49] In both techniques, the overall spectral shape is consistent with a diradical species. While cw-EPR spectroscopy detects the first derivative of the absorption spectrum, pulsed EPR spectroscopy provides the absorption spectrum directly. Integrating the pulsed EPR spectrum yields an intensity equivalent to the doubly integrated cw-EPR signal. When we plot the intensity of the EPR signal multiplied by the temperature ($I \times T$) as a function of temperature, the intensity remains largely constant across the measured temperature range, showing no systematic variation and only minor scatter (see Fig. 2d and e). The close similarity of the values strongly indicates that the singlet and triplet energy levels are effectively degenerate. This conclusion is further supported by DFT calculations, which predict near-degeneracy of the singlet and triplet states (see Table S1 in the SI). For the non-chiral pseudo-*p*-PCP-TTM$_2$, no complex coupling patterns are visible in the EPR spectrum (see Fig. 2a). This absence of coupling can be explained by the radical–radical distance of 1.92 nm (obtained by the DFT calculation), which is very large compared to the 0.76 nm obtained for pseudo-*o*-PCP-TTM$_2$. Effectively, in pseudo-*p*-PCP-TTM$_2$, the distance between the radical centers is too large for interaction. While performing vt-EPR measurements for pseudo-*p*-PCP-TTM$_2$ in frozen toluene, we do not observe any systematic correlation between the signal intensity and the temperature (see Fig. S1 in the SI). In conclusion, pseudo-*p*-PCP-TTM$_2$ is a biradical with isolated spins that are best described as separated doublet species.

Optical characterization and TD-DFT calculations

The UV-vis absorption spectra of pseudo-*o*-PCP-TTM$_2$, pseudo-*p*-PCP-TTM$_2$, and Ph-TTM exhibit similar features, with an intense absorption band in the near UV region (with a maximum at $\lambda_{abs} \approx 375$ nm), an absorption or shoulder at $\lambda_{abs} \approx 415$ nm and broad absorption bands in the visible range, as is typical for the TTM radical and its derivatives (see Fig. 3a).[7,8,50] Moreover, we observe absorption bands around $\lambda_{abs} \approx 300$ nm as well as at $\lambda_{abs} \approx 436$ nm and $\lambda_{abs} \approx 440$ nm for pseudo-*o*- and pseudo-*p*-PCP-TTM$_2$, respectively. We assign the band at $\lambda_{abs} \approx 415$ nm to an absorption associated with the TTM-ethynylene-PCP or TTM-ethynylene-phenyl bridge, since this feature is prominent in all samples and cannot be assigned to the other individual molecular building blocks. The bands at 436 nm and 440 nm, respectively, for the two diradicals, are attributed to extended π-conjugation and through-space electronic interactions involving the [2.2]paracyclophane core and the conjugated ethynylene-TTM units, resulting in a red-shifted transition relative to the individual components (see Fig. 3a). Similar acceptor functionalized PCPs also show this bathochromic shift through extended π-conjugation across the ethynylene bridges and substantial through-space conjugation into the other PCP deck.[34,51–54] To understand the transitions in the visible spectrum better, we perform time-dependent (TD)-DFT at the UB3LYP/def2-SVPD level of theory using the above optimized ground state geometries. We compute the natural transition orbitals (NTOs) for the lowest energy transitions for the three molecules. This analysis allows us to assign NTOs to the absorption bands at 436 nm and 440 nm in the pseudo-*o*- and pseudo-*p*-PCP-TTM$_2$, where we observe the expected CT and through-space delocalization of the hole across the two PCP decks, whereas the electron resides predominantly on the TTM unit, corroborating our above interpretation (see Fig. S14). Since the diradicals are symmetric, we observe isoenergetic $S_0 \rightarrow S_1$ and $S_0 \rightarrow S_2$ transitions. When we inspect the NTOs, we observe charge transfer (CT) transitions for these $S_0 \rightarrow S_1$ and $S_0 \rightarrow S_2$ transitions with the lowest energies. Since the pseudo-*o*-PCP-TTM$_2$ and the pseudo-*p*-PCP-TTM$_2$ are symmetric, the NTOs for the S_1 and S_2 transitions are mirror images, which is why we only display one of the two mirroring states and only the state with the greatest contribution to the transition (see Fig. 3b). The full set of NTOs is displayed in Fig. S13 in the SI. The next transition for the two diradicals is the T_1 transition at slightly higher energy. When inspecting the corresponding NTOs, it becomes apparent that the T_1 transitions exhibit hybridized local and charge transfer (HLCT) character. It should be noted that the NTO of the D_1 transition of the Ph-TTM monoradical is very similar to the NTO of the T_1 transition of pseudo-*p*-PCP-TTM$_2$ (see Fig. 3a). While the computed λ_{abs} values of the T_1 transitions of the diradicals are similar in energy (588 nm and 589 nm), the S_1/S_2 transitions differ in their energy. For the S_1/S_2 transition, pseudo-*o*-PCP-TTM$_2$ exhibits λ_{abs} = 726 nm and for the pseudo-*p*-PCP-TTM$_2$, λ_{abs} = 670 nm

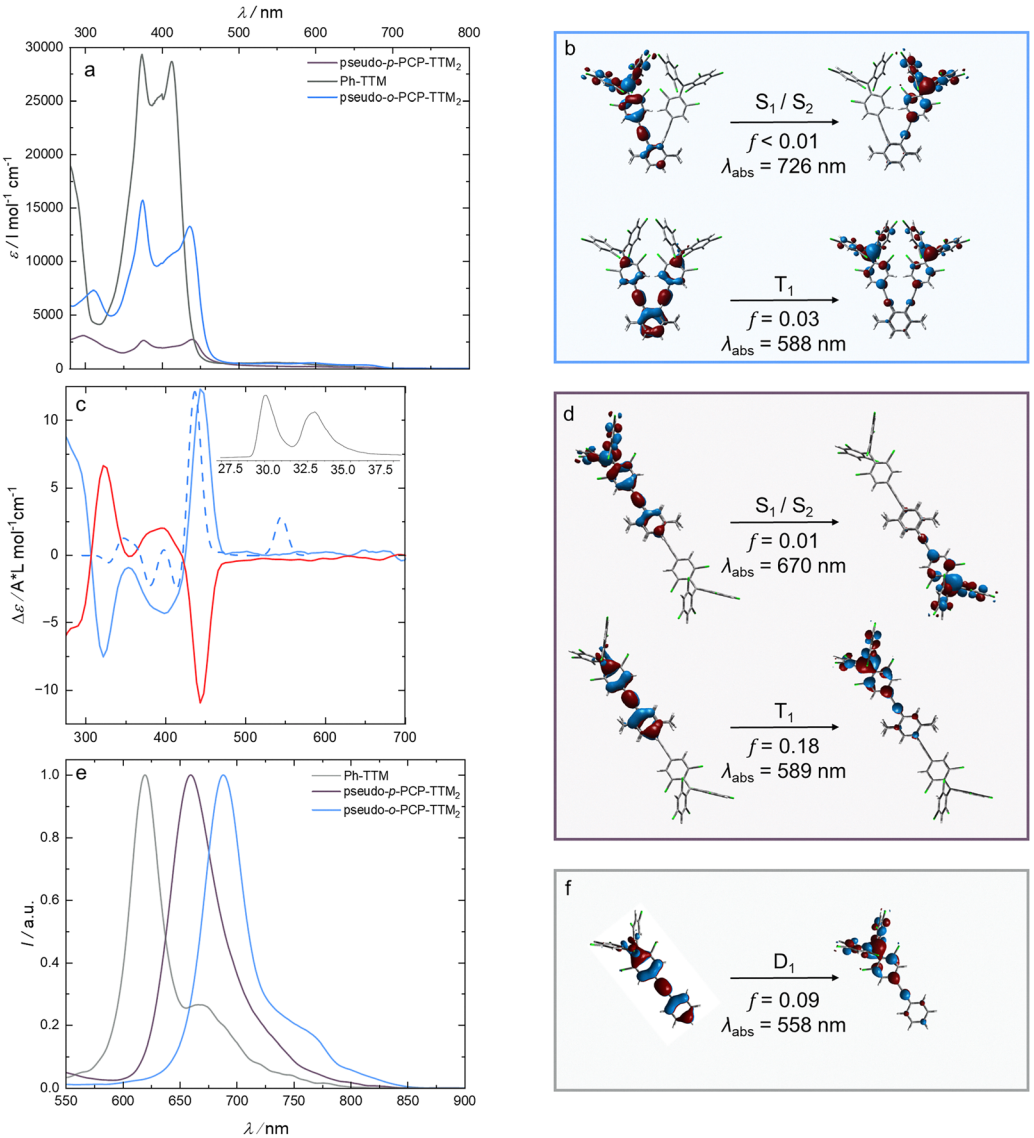

Fig. 3 (a) Normalized absorption spectra of pseudo-*o*-PCP-TTM$_2$ (blue), pseudo-*p*-PCP-TTM$_2$ (violet) and Ph-TTM (grey) in cyclohexane solutions ($c = 10^{-5}$ M). (b) Hole (h^+) and electron (e^-) natural transition orbitals (NTOs) for the $S_0 \rightarrow S_{1/2}$ and $T_0 \rightarrow T_1$ transitions in pseudo-*o*-PCP-TTM$_2$, calculated at the UB3LYP/def2-SVPD level of theory. (c) CD spectra of the R_p (blue) and S_p (red) enantiomers with a comparison to the theoretical CD spectrum of the R_p enantiomer (dashed lines) and a chiral HPLC elugram of pseudo-*o*-PCP-TTM$_2$ (inset). (d) Hole (h^+) and electron (e^-) natural transition orbitals (NTOs) for the $S_0 \rightarrow S_{1/2}$ and $T_0 \rightarrow T_1$ transitions in pseudo-*p*-PCP-TTM$_2$, calculated at the UB3LYP/def2-SVPD level of theory. (e) Normalized emission spectra in cyclohexane of pseudo-*o*-PCP-TTM$_2$ (blue), pseudo-*p*-PCP-TTM$_2$ (violet) and Ph-TTM (grey) ($c = 10^{-5}$ M). (f) Hole (h^+) and electron (e^-) natural transition orbitals (NTOs) for the $D_0 \rightarrow D_1$ of Ph-TTM, calculated at the UB3LYP/def2-SVPD level of theory.

(see Fig. 3b and d). This computed bathochromic shift in the S_1/S_2 transition of the pseudo-*o*-PCP-TTM$_2$ compared to the pseudo-*p*-PCP-TTM$_2$ can also explain why the chiral pseudo-*o*-PCP-TTM$_2$ diradical exhibits the most red-shifted photoluminescence (see Fig. 3e). The emission will most likely occur from the transition with the smallest energy gap (Kasha's rule), which is why the S_1/S_2 energies are important for the emission process ($S_1/S_2 \rightarrow S_0$). By contrast, Ph-TTM only exhibits a lowest excited D_1 state, which is energetically most similar to the T_1 in the diradicals (see Fig. 3f). This explains why we observe the most blue-shifted emission from the monoradical (see Fig. 3e).

The photoluminescence quantum yield of the diradicals is rather low at $\phi \approx 1\%$, which is common for alternant TTM-based diradicals due to their symmetry breaking charge separation upon excitation.[14] Moreover, the balance between donor and TTM acceptor strengths in the Ph-TTM monoradicals does not seem to be ideal, as we obtain only slightly higher $\phi = 1.2\%$. Excitation spectra recorded at the maximum photoluminescence wavelength (λ_{PL}) of the two diradical species closely resemble the corresponding UV-vis absorption profiles, confirming that the observed low photoluminescence indeed originates from the diradicals rather than from emissive impurities (see Fig. S8, SI).

To elucidate the chiroptical properties of the chiral diradical, we first resolve the racemic mixture of pseudo-*o*-PCP-TTM$_2$ into the planar chiral enantiomers (with regard to the PCP unit) using chiral high-performance liquid chromatography (HPLC). We obtain an almost baseline separation between the HPLC peaks on a chiral Lux® i-Amylose-3 column, allowing us to isolate the corresponding enantiomers (see HPLC trace in the inset of Fig. 3c). We investigate the pseudo-*o*-PCP-TTM$_2$ enantiomers using circular dichroism (CD) spectroscopy.

Mirror-image CD spectra are obtained for the two enantiomers. We can clearly observe the Cotton effect in the CD spectrum at λ_{abs} = 314 nm and 436 nm, originating from the PCP unit. The spectrum drawn in red is subject to the positive Cotton effect, since we have a positive $\Delta\varepsilon$ below the λ_{abs} and at longer wavelengths, $\Delta\varepsilon$ is negative. Conversely, the spectrum drawn in blue is subject to the negative Cotton effect (see Fig. 3c). The dissymmetry factor g_{abs} is determined to be 2.1×10^{-4}, which is in the same range as that of other substituted [2.2]PCPs.[25,34] By comparing the theoretical CD spectrum (obtained by TD-DFT) with the experimental data, the blue curve in Fig. 3c can be assigned to the R_p enantiomer, and the red curve can be assigned to the S_p enantiomer. Unfortunately, the ϕ is too low to determine a dissymmetry factor for the circularly polarized emission CPL ($g_{lum} < 10^{-4}$) (see Fig. S7 in the SI).

Conclusions

In this work, we have successfully synthesized a novel chiral pseudo-*ortho*-PCP-TTM$_2$ diradical species, with degenerate singlet and triplet ground states with ZFS. The chiral diradical can be enantiomerically resolved and the enantiomers show strong CD though weak photoluminescence. Further research should focus on increasing ϕ, for example, by introduction of electron donor moieties, such as carbazole.[55] To optimize the application in the field of quantum information processing or for quantum sensors in general, it could also be interesting to stabilize the triplet ground state against the singlet state to avoid the population of the latter at room temperature. We anticipate that these results will inspire further exploration of molecular architectures with tailored spin-state landscapes, advancing both the understanding and application of organic open-shell systems.

Author contributions

L. S. carried out the synthesis and characterization of the compounds. A. J. C. K. and H. F. B. conceptualized the project. M. E. A. supervised the project. M. R. R. synthesized PCP starting materials. R. B. and F. J. conducted EPR experiments and analysis. M. G. carried out the enantiomeric separation and CD spectroscopy. J. Z. performed (TD)-DFT calculations. F. J., H. F. B., and A. J. C. K. provided supervision, infrastructure, and secured funding. L. S. and A. J. C. K. wrote the first draft and all authors revised and edited the manuscript.

Conflicts of interest

There are no conflicts to declare.

Data availability

The data for this article, including DFT and TD-DFT, are available at zenodo.org at https://doi.org/10.5281/zenodo.17301951.

All other data supporting this article have been included as part of the supplementary information (SI). Supplementary information is available. See DOI: https://doi.org/10.1039/d5tc02343b.

Acknowledgements

The authors thank Michael Baumann (at Uni Ulm) for his support in measuring photoluminescence quantum yields. J. Z. acknowledges IQST for a PhD program within the IQST Graduate School @QuantumBW supported by the Baden-Württemberg Ministry of Science, Research, and Arts. The authors acknowledge support from the state of Baden-Württemberg through bwHPC and the Deutsche Forschungsgemeinschaft (DFG, German Research Foundation), project number: INST 40/575-1 FUGG (JUSTUS 2 cluster), and the DFG for funding through project numbers: 500226157, 445471845, 445471097, 445470598, and 417643975.

References

1 M. Abe, Diradicals, *Chem. Rev.*, 2013, **113**(9), 7011–7088.
2 D. Straub, M. Gross, M. E. Arnold, J. Zolg and A. J. C. Kuehne, On the photoluminescence in triarylmethyl-centered mono-, di-, and multiradicals, *Beilstein J. Org. Chem.*, 2025, **21**(1), 964–998.
3 D. Shimizu, H. Sotome, H. Miyasaka and K. Matsuda, Optically Distinguishable Electronic Spin-isomers of a Stable Organic Diradical, *ACS Cent. Sci.*, 2024, **10**(4), 890–898.
4 W. B. Sparks, J. Hough, T. A. Germer, F. Chen, S. DasSarma, P. DasSarma and W. Martin, *et al.*, Detection of circular polarization in light scattered from photosynthetic microbes, *Proc. Natl. Acad. Sci. U. S. A.*, 2009, **106**(19), 7816–7821.
5 A. Shimizu, T. Morikoshi, K. Sugisaki, D. Shiomi, K. Sato, T. Takui and R. Shintani, Synthesis and isolation of a kekule hydrocarbon with a triplet ground state, *Angew. Chem.*, 2022, **134**(29), e202205729.
6 C. Shu, Z. Yang and A. Rajca, From stable radicals to thermally robust high-spin diradicals and triradicals, *Chem. Rev.*, 2023, **123**(20), 11954–12003.
7 D. Velasco, S. Castellanos, M. López, F. López-Calahorra, E. Brillas and L. Juliá, Red organic light-emitting radical adducts of carbazole and tris (2, 4, 6-trichlorotriphenyl) methyl radical that exhibit high thermal stability and electrochemical amphotericity, *J. Org. Chem.*, 2007, **72**(20), 7523–7532.

8 X. Ai, E. W. Evans, S. Dong, A. J. Gillett, H. Guo, Y. Chen and F. Li, *et al.*, Efficient radical-based light-emitting diodes with doublet emission, *Nature*, 2018, **563**(7732), 536–540.
9 Z. Cui, A. Abdurahman, X. Ai and F. Li, Stable luminescent radicals and radical-based LEDs with doublet emission, *CCS Chem.*, 2020, **2**(4), 1129–1145.
10 K. Matsuda, R. Xiaotian, K. Nakamura, M. Furukori, T. Hosokai, K. Anraku and K. Albrecht, *et al.*, Photostability of luminescent tris (2, 4, 6-trichlorophenyl) methyl radical enhanced by terminal modification of carbazole donor, *Chem. Commun.*, 2022, **58**(97), 13443–13446.
11 R. G. Hicks, What's new in stable radical chemistry?, *Org. Biomol. Chem.*, 2007, **5**(9), 1321–1338.
12 C. Lu, E. Cho, Z. Cui, Y. Gao, W. Cao, J. L. Brédas and F. Li, *et al.*, Towards efficient and stable donor-acceptor luminescent radicals, *Adv. Mater.*, 2023, **35**(6), 2208190.
13 M. E. Arnold, L. Roß, P. Thielert, F. Bartley, J. Zolg, F. Bartsch and A. J. Kuehne, *et al.*, On the Effect of Donor Strength on the Photoluminescence Performance in Mono-Substituted N-Donor Triarylmethyl Radicals, *Adv. Opt. Mater.*, 2024, **12**(22), 2400697.
14 X. Chang, M. E. Arnold, R. Blinder, J. Zolg, J. Wischnat, J. van Slageren and M. von Delius, *et al.*, A stable chichibabin diradicaloid with near-infrared emission, *Angew. Chem., Int. Ed.*, 2024, **63**(29), e202404853.
15 Z. Zhu, Z. Kuang, L. Shen, S. Wang, X. Ai, A. Abdurahman and Q. Peng, Dual Channel Emissions of Kasha and Anti-Kasha from a Single Radical Molecule, *Angew. Chem.*, 2024, **136**(42), e202410552.
16 A. Abdurahman, J. Wang, Y. Zhao, P. Li, L. Shen and Q. Peng, A highly stable organic luminescent diradical, *Angew. Chem., Int. Ed.*, 2023, **62**(15), e202300772.
17 D. Schäfter, J. Wischnat, L. Tesi, J. A. De Sousa, E. Little, J. McGuire and J. Van Slageren, *et al.*, Molecular one-and two-qubit systems with very long coherence times, *Adv. Mater.*, 2023, **35**(38), 2302114.
18 Y. Su, X. Wang, L. Wang, Z. Zhang, X. Wang, Y. Song and P. P. Power, Thermally controlling the singlet–triplet energy gap of a diradical in the solid state, *Chem. Sci.*, 2016, **7**(10), 6514–6518.
19 M. R. Wasielewski, M. D. Forbes, N. L. Frank, K. Kowalski, G. D. Scholes, J. Yuen-Zhou and K. B. Whaley, *et al.*, Exploiting chemistry and molecular systems for quantum information science, *Nat. Rev. Chem.*, 2020, **4**(9), 490–504.
20 D. Mesto, M. Orza, B. Bardi, A. Punzi, I. Ratera, J. Veciana and F. Negri, *et al.*, Luminescent Trityl-based Diradicaloids: A Theoretical and Experimental Assessment of Charge-Resonance in Low-Lying Excited States, *Chem. – Eur. J.*, 2025, **31**(23), e202500749.
21 S. M. Kopp, S. Nakamura, B. T. Phelan, Y. R. Poh, S. B. Tyndall, P. J. Brown and M. R. Wasielewski, *et al.*, Luminescent organic triplet diradicals as optically addressable molecular qubits, *J. Am. Chem. Soc.*, 2024, **146**(40), 27935–27945.
22 N. V. Vorontsova, V. I. Rozenberg, E. V. Sergeeva, E. V. Vorontsov, Z. A. Starikova, K. A. Lyssenko and H. Hopf, Symmetrically Tetrasubstituted [2.2] Paracyclophanes: Their Systematization and Regioselective Synthesis of Several Types of Bis-Bifunctional Derivatives by Double Electrophilic Substitution, *Chem. – Eur. J.*, 2008, **14**(15), 4600–4617.
23 K. Reznikova, C. Hsu, W. M. Schosser, A. Gallego, K. Beltako, F. Pauly and M. Mayor, *et al.*, Substitution pattern controlled quantum interference in [2.2] paracyclophane-based single-molecule junctions, *J. Am. Chem. Soc.*, 2021, **143**(34), 13944–13951.
24 S. Felder, S. Wu, J. Brom, L. Micouin and E. Benedetti, Enantiopure planar chiral [2.2] paracyclophanes: Synthesis and applications in asymmetric organocatalysis, *Chirality*, 2021, **33**(9), 506–527.
25 S. Felder, M. L. Delcourt, D. Contant, R. Rodríguez, L. Favereau, J. Crassous and E. Benedetti, *et al.*, Compact CPL emitters based on a [2.2] paracyclophane scaffold: recent developments and future perspectives, *J. Mater. Chem. C*, 2023, **11**(6), 2053–2062.
26 Z. Hassan, E. Spuling, D. M. Knoll and S. Bräse, Regioselektive Funktionalisierung von [2.2] Paracyclophanen: aktuelle Synthesefortschritte und Perspektiven, *Angew. Chem.*, 2020, **132**(6), 2176–2190.
27 H. Han, D. Zhang, Z. Zhu, R. Wei, X. Xiao, X. Wang and D. Zhao, *et al.*, Aromatic stacking mediated spin–spin coupling in cyclophane-assembled diradicals, *J. Am. Chem. Soc.*, 2021, **143**(42), 17690–17700.
28 R. Matsuoka, S. Kimura, T. Miura, T. Ikoma and T. Kusamoto, Single-molecule magnetoluminescence from a spatially confined persistent diradical emitter, *J. Am. Chem. Soc.*, 2023, **145**(25), 13615–13622.
29 J. Duan, Y. Shi, F. Zhao, C. Li, Z. Duan, N. Zhang and P. Chen, Chiral Luminescent Aza [7] helicenes Functionalized with a Triarylborane Acceptor and Near-Infrared-Emissive Doublet-State Radicals, *Inorg. Chem.*, 2023, **62**(39), 15829–15833.
30 M. Gross, F. Zhang, M. E. Arnold, P. Ravat and A. J. Kuehne, Aza [7] helicene Functionalized Triphenylmethyl Radicals with Circularly Polarized Doublet Emission, *Adv. Opt. Mater.*, 2024, **12**(4), 2301707.
31 P. Mayorga-Burrezo, V. G. Jiménez, D. Blasi, T. Parella, I. Ratera, A. G. Campaña and J. Veciana, An Enantiopure Propeller-Like Trityl-Brominated Radical: Bringing Together a High Racemization Barrier and an Efficient Circularly Polarized Luminescent Magnetic Emitter, *Chem. – Eur. J.*, 2020, **26**(17), 3776–3781.
32 Y. Hattori, R. Matsuoka, A. Baba, S. Yoshida, M. Yamada, R. Fujita and T. Kawai, *et al.*, A Luminescent Stable Triarylmethyl Diradical with an Axially Chiral Spacer, *Chem. – Eur. J.*, 2025, **31**(21), e202500284.
33 H. Guo, J. B. Lovell, C. Shu, M. Pink, M. Morton, S. Rajca and A. Rajca, Chiral π-Conjugated Double Helical Aminyl Diradical with the Triplet Ground State, *J. Am. Chem. Soc.*, 2024, **146**(13), 9422–9433.
34 M. R. Rapp, W. Leis, F. Zinna, L. Di Bari, T. Arnold, B. Speiser and H. F. Bettinger, *et al.*, Bright Luminescence

by Combining Chiral [2.2] Paracyclophane with a Boron–Nitrogen-Doped Polyaromatic Hydrocarbon Building Block, *Chem. – Eur. J.*, 2022, **28**(11), e202104161.

35 M. E. Arnold and A. J. Kuehne, (2,6-Dichloro-4-iodophenyl) bis (2,4,6-trichlorophenyl) methane as a precursor in efficient cross-coupling reactions for donor and acceptor functionalized triphenylmethyl radicals, *Dyes Pigm.*, 2023, **208**, 110863.

36 M. Trunk, A. Herrmann, H. Bildirir, A. Yassin, J. Schmidt and A. Thomas, Copper-Free Sonogashira Coupling for High-Surface-Area Conjugated Microporous Poly (aryleneethynylene) Networks, *Chem. – Eur. J.*, 2016, **22**(21), 7179–7183.

37 K. E. Preuss, Pancake bonds: π-Stacked dimers of organic and light-atom radicals, *Polyhedron*, 2014, **79**, 1–15.

38 Q. Xiang, J. Guo, J. Xu, S. Ding, Z. Li, G. Li and Z. Sun, *et al.*, Stable olympicenyl radicals and their π-dimers, *J. Am. Chem. Soc.*, 2020, **142**(25), 11022–11031.

39 O. Armet, J. Veciana, C. Rovira, J. Riera, J. Castaner, E. Molins and J. Brichfeus, *et al.*, Inert carbon free radicals. 8. Polychlorotriphenylmethyl radicals: synthesis, structure, and spin-density distribution, *J. Phys. Chem.*, 1987, **91**(22), 5608–5616.

40 C. E. Tait, M. D. Krzyaniak and S. Stoll, Computational tools for the simulation and analysis of spin-polarized EPR spectra, *J. Magn. Reson.*, 2023, **349**, 107410.

41 S. Stoll and A. Schweiger, EasySpin, a comprehensive software package for spectral simulation and analysis in EPR, *J. Magn. Reson.*, 2006, **178**(1), 42–55.

42 O. Schiemann and T. F. Prisner, Long-range distance determinations in biomacromolecules by EPR spectroscopy, *Q. Rev. Biophys.*, 2007, **40**(1), 1–53.

43 G. Jeschke, Determination of the nanostructure of polymer materials by electron paramagnetic resonance spectroscopy, *Macromol. Rapid Commun.*, 2002, **23**(4), 227–246.

44 S. Richert, C. E. Tait and C. R. Timmel, Delocalisation of photoexcited triplet states probed by transient EPR and hyperfine spectroscopy, *J. Magn. Reson.*, 2017, **280**, 103–116.

45 X. Guo, Y. Li, Z. Yao, C. Jia and L. Zhang, Spin chirality driven by the Dzyaloshinskii–Moriya interaction in one-dimensional antiferromagnetic chain, *AIP Adv.*, 2023, **13**(4), 045103.

46 P. Garbacz and J. Vaara, *Chirality-sensitive Effects Induced by Antisymmetric Spin–Spin Coupling*, 2024.

47 R. J. Elliott, Theory of the effect of spin-orbit coupling on magnetic resonance in some semiconductors, *Phys. Rev.*, 1954, **96**(2), 266.

48 A. M. Tyryshkin, S. A. Lyon, A. V. Astashkin and A. M. Raitsimring, Electron spin relaxation times of phosphorus donors in silicon, *Phys. Rev. B: Condens. Matter Mater. Phys.*, 2003, **68**(19), 193207.

49 A. A. Kuzhelev, D. V. Trukhin, O. A. Krumkacheva, R. K. Strizhakov, O. Y. Rogozhnikova, T. I. Troitskaya and E. G. Bagryanskaya, *et al.*, Room-temperature electron spin relaxation of triarylmethyl radicals at the X-and Q-bands, *J. Phys. Chem. B*, 2015, **119**(43), 13630–13640.

50 K. Nakamura, K. Matsuda, R. Xiaotian, M. Furukori, S. Miyata, T. Hosokai and K. Albrecht, *et al.*, Effects of halogen atom substitution on luminescent radicals: a case study on tris (2, 4, 6-trichlorophenyl) methyl radical-carbazole dyads, *Faraday Discuss.*, 2024, **250**, 192–201.

51 S. Lambud, A. Bhadke, Z. A. Siddiqui, V. Chaudhari, N. Sekar, R. Bhosale and S. More, Synthesis and Optical Property Modulation of Substituted [2.2] Paracylophanes through Through-Space Conjugation, *Eur. J. Org. Chem.*, 2024, e202400360.

52 L. Lin, Y. Morisaki and Y. Chujo, New Type of Donor-Acceptor Through-Space Conjugated Polymer, *Int. J. Polym. Sci.*, 2010, **2010**(1), 908128.

53 H. Maeda, R. Inoue, A. Saeki and Y. Morisaki, Synthesis of optically active through-space conjugated polymers consisting of planar chiral pseudo-meta-disubstituted [2.2] Paracyclophane, *Polym. J.*, 2023, **55**(4), 537–545.

54 L. Lin, Y. Morisaki and Y. Chujo, Synthesis of through-space conjugated polymers containing [2.2] paracyclophane and thieno [3,4-*b*] pyrazine in the main chain, *J. Polym. Sci., Part A: Polym. Chem.*, 2009, **47**(24), 7003–7011.

55 V. C. Wakchaure, X. Chang, J. Zolg, R. Blinder, M. E. Arnold, F. Jelezko and M. von Delius, *et al.*, Carbazole-functionalized Chichibabin diradicaloids with redshifted absorption and enhanced photoluminescence, *Chem. Commun.*, 2025, **61**(49), 8855–8858.